Dynamic Visual Dominance in Stereoscopic Foveation

DANIEL JIMÉNEZ-NAVARRO*, Max Planck Institute for Informatics, Germany
COLIN GROTH, New York University, USA
KENNETH CHEN, New York University, USA
QI SUN, New York University, USA
KAROL MYSZKOWSKI, Max Planck Institute for Informatics, Germany
HANS-PETER SEIDEL, Max Planck Institute for Informatics, Germany
ANA SERRANO, University of Zaragoza - I3A, Spain

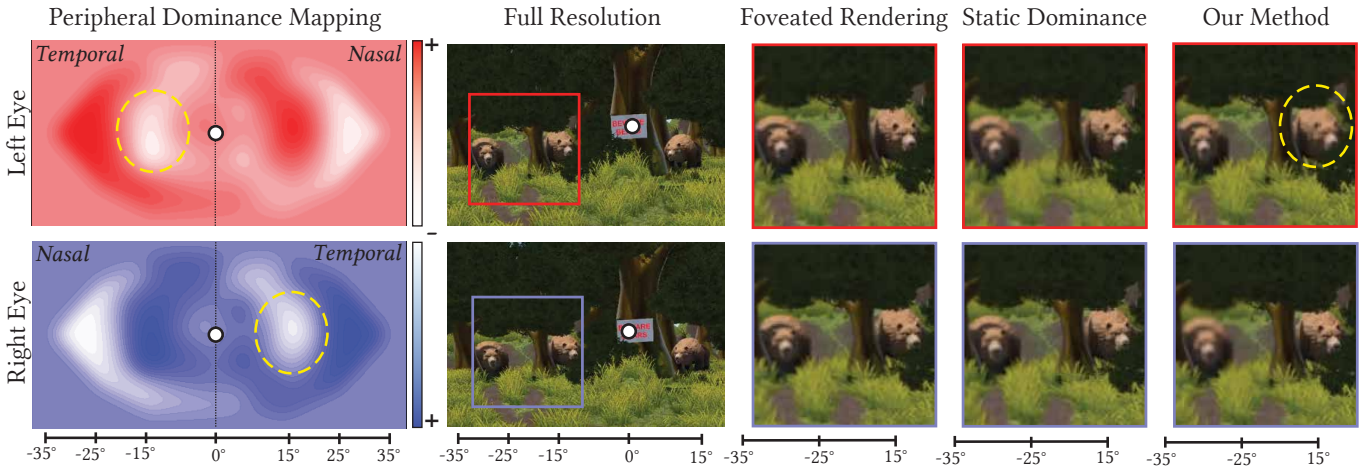

Fig. 1. We show that visual dominance is not a static, eye-fixed percept, but varies dynamically between the eyes as a function of gaze direction and peripheral offset from the fovea. Consequently, different regions of a stereoscopic image are dominated by different eyes depending on the fixation point. **Left:** Our retinal dominance maps for the left and right eyes obtained from our psychophysical experiments. The central white markers indicate the fixation point, and the bottom scale denotes retinal eccentricity. Red and blue colors indicate the level of dominance toward the left and right eyes, respectively. As can be observed, the temporal viewing hemifield (corresponding to the nasal retinal region) consistently dominates over the nasal viewing hemifield (corresponding to the temporal retinal region), particularly at larger eccentricities, with the exception of the blind spots (dashed circles). **Right:** We leverage the map to introduce asymmetric blur for foveated rendering. With standard foveated rendering as reference, the first approach applies a static dominance, introducing additional blur in the left eye only, assuming right-eye dominance. Our method, shown in the last column, accounts for dynamic dominance changes by applying additional blur according to the dynamic dominance maps of each eye. Please refer to the difference in blurriness between the two bears for better visualization. While the static approach applies a stronger blur to the nominally non-dominant left eye, the dominance maps reveal a local dominance switch in this region, which can lead to visible artifacts. In contrast, our method adapts to this switch, shifting additional blur between eyes where it is perceptually less noticeable. By leveraging gaze-dependent, dynamically varying visual dominance, our approach enables stronger localized blur with reduced artifacts.

In human vision, the inputs perceived by each eye do not contribute equally to the final percept. Instead, visual dominance influences how these inputs are fused, giving more weight to one eye view over the other. While eye dominance has been traditionally treated as a static, eye-fixed property, recent evidence suggests that dominance can vary with viewing conditions. In this work, we systematically characterize dynamic visual dominance across the visual field, with a particular focus on peripheral vision, where perceptual asymmetries are most relevant for stereoscopic rendering. Through two complementary psychophysical experiments, we first show that tolerance to eye-asymmetric blur at the fovea under binocular viewing depends on gaze direction, confirming that eye dominance is not spatially invariant. We then show that peripheral dominance is primarily governed by retinal eccentricity, with consistent naso-temporal asymmetries and dominance reversals around the blind spots. We leverage our insights in a dominance-contingent rendering application, where additional blur is selectively applied to the perceptually non-dominant eye regions under binocular viewing. Compared to static dominance approaches, our method enables stronger localized quality reductions, illustrating the practical relevance of dynamic peripheral

*Corresponding Author.

Authors' Contact Information: Daniel Jiménez-Navarro, djimenez@mpi-inf.mpg.de, Max Planck Institute for Informatics, Germany; Colin Groth, c.groth@nyu.edu, New York University, USA; Kenneth Chen, kennychen@nyu.edu, New York University, USA; Qi Sun, qisun@nyu.edu, New York University, USA; Karol Myszkowski, karol@mpi-inf.mpg.de, Max Planck Institute for Informatics, Germany; Hans-Peter Seidel, hpseidel@mpi-inf.mpg.de, Max Planck Institute for Informatics, Germany; Ana Serrano, anase@unzar.es, University of Zaragoza - I3A, Spain.

SIGGRAPH Conference Papers '26, Los Angeles, CA, USA

ACM ISBN 979-8-4007-2554-8/2026/07
https://doi.org/10.1145/3799902.3811164

dominance for stereoscopic foveated rendering. Thus, our goal through this work is to show how visual dominance behaves dynamically in both the fovea and the periphery, indicating how foveation techniques could benefit from it.

CCS Concepts: • **Computing methodologies** → **Virtual reality**; **Perception**.

ACM Reference Format:
Daniel Jiménez-Navarro, Colin Groth, Kenneth Chen, Qi Sun, Karol Myszkowski, Hans-Peter Seidel, and Ana Serrano. 2026. Dynamic Visual Dominance in Stereoscopic Foveation. In *Special Interest Group on Computer Graphics and Interactive Techniques Conference Conference Papers (SIGGRAPH Conference Papers '26), July 19–23, 2026, Los Angeles, CA, USA.* ACM, New York, NY, USA, 11 pages. https://doi.org/10.1145/3799902.3811164

1 Introduction

Human visual perception emerges from the fusion of the two retinal images captured by the eyes while binocular fusion denotes the neural mechanism that combines these two signals into a single percept. In stereoscopic vision, a clear percept arises when corresponding retinal locations in both eyes receive similar visual information. Small interocular differences, however, can be compensated without conscious awareness, enabling perceptual stability despite local mismatches between the two inputs. Similar to handedness, most individuals exhibit ocular dominance, where one eye contributes more strongly to the integrated percept. Approximately, $70-80\%$ of the population is right-eye dominant [Chaurasia and Mathur 1976]. During binocular fusion of corresponding retinal regions, signals from the dominant eye receive greater perceptual weight. As a consequence, attenuating high-frequency content in the non-dominant eye, such as through display-side blurring, can still yield a clear fused percept. Computer graphics has exploited this property by interpreting blur as a reduced sampling density requirement in ray tracing or variable rate shading (VRS).

Classical gaze-contingent rendering relies on the non-uniform distribution of photoreceptors across the visual field and reduces sampling density in peripheral regions to improve computational efficiency [Patney et al. 2016]. Extending this concept, prior work has investigated eye dominance for enhanced efficiency in stereoscopic displays [Meng et al. 2020; Wang et al. 2023]. These approaches apply a fixed blur increment to the non-dominant eye and assume that eye dominance is static in magnitude and constant in eye assignment. However, eye dominance is not a fixed characteristic but a dynamic effect that adapts with perceptual context [Prummer et al. 2025].

As shown in Fig. 1, we investigate and quantify how eye dominance shifts according to gaze position and eccentricity. Our psychophysical experiments show that the dominance is more dynamic and adaptive than commonly assumed in graphics applications, offering key insights for advancing stereoscopic gaze-contingent rendering. *First*, our results reveal how foveal eye dominance depends on gaze position in pure visual acuity tasks. That is, when focusing on a specific region, the same eye will always be dominant in this region, making the pre-computation of rendering effects possible. As expected, stimuli presented in the right visual field tend to be dominated by the right eye, and vice versa. *Second*, as stimuli shift towards the periphery, eye dominance and its strength depend mainly on eccentricity. Based on the results, we derive a dominance map that guides peripheral blur levels relatively to the observer's gaze position.

Our findings offer potential implications for real-time stereoscopic rendering. In this direction, we apply our dominance map through rendering shaders to show the potential of enhancing foveated rendering with improved fidelity and reduced display power consumption. Our contributions are summarized as follows:

- We characterize visual dominance shifts in the fovea as a function of gaze direction, and show that tolerance to eye-asymmetric blur under binocular viewing exceeds binocular blur detection thresholds, particularly when applied to the non-dominant eye.
- We show that transitions in peripheral dominance are driven by naso-temporal asymmetry and the eyes' blind spots.
- We apply our insights to a proof-of-concept gaze-contingent rendering application, improving over a static dominance alternative.

2 Related Work

2.1 Stereoscopic Perception and Fusion

Stereoscopic perception (stereopsis) arises from the coherent integration of the two retinal images into a single percept [Cang et al. 2023; Jiménez-Navarro et al. 2026], a process known as binocular fusion [Sperling 1970]. Binocular fusion is possible only when visual signals fall on corresponding retinal locations, a condition that is typically satisfied when the object lies within or close to the focused depth [Sperling 1970]. The overlapping binocular field, within which both retinas receive information from the same region of space, spans approximately 110° horizontally [Stidwill and Fletcher 2017]; outside this region, vision is monocular and cannot support stereopsis.

While the human visual system can tolerate small interocular differences in sharpness, larger blur disparities typically induce interocular blur suppression, whereby the sharper retinal image dominates the percept by suppressing high-frequency content from the blurred eye [Georgeson and Wallis 2014]. When interocular differences become too pronounced, stable fusion may break down and transition into binocular rivalry, characterized by temporal alternations between monocular percepts [Arnold et al. 2007]. At the same time, controlled differential blur can act as an important depth-of-field cue that assists binocular correspondence and reduces rivalry in complex scenes [Hoffman and Banks 2010].

2.2 Eye Dominance

Eye dominance describes the preferential weighting of one eye's input during binocular integration of discrepant images and primarily affects overlapping binocular regions. Reported statistics suggesting that approximately 70–80% of the population is right-eye dominant are typically derived from tasks with centrally positioned stimuli, where the notion of eyedness [Chaurasia and Mathur 1976] remains stable in high-precision frontal positioning tasks such as target aiming, and shows no consistent alignment with hand or foot preference [Carey and Hutchinson 2013; Chaurasia and Mathur 1976].

Subsequent work demonstrates that this static notion of eye dominance is incomplete. Khan and Crawford [2001] showed that *sighting dominance* (SD) switches dynamically between the eyes depending on horizontal gaze angle in a reach–grasp task: For observers with

right-eye dominance, dominance reversals occurred when targets were placed in the left visual hemifield (i.e., on the side opposite to the dominant eye) at eccentricities exceeding 15.5°, while observers with left-eye dominance exhibited corresponding switches for targets placed in the right visual hemifield. These gaze-dependent dominance changes are consistent with relative image size effects favoring the eye closer to the target [Banks et al. 2004]. Such gaze-dependent behavior was confirmed across standard clinical tests by Quartley and Firth [2004]. Complementary studies on *sensory eye dominance* (SED), where discrepant content is directly projected to corresponding retinal locations, report a naso–temporal asymmetry favoring the temporal visual hemifield (nasal retina) at eccentricities above 20° [Fahle 1987; Fahle and Schmid 1988], and below 4° [Stanley et al. 2011, 2019]. These effects are commonly attributed to asymmetries in photoreceptor and ganglion cell density and cortical representation, with more recent work reporting deviations at eccentricities below 10° [Paffen 2025], substantial inter-subject variability [Chaumillon et al. 2017], and differences between laboratory and real-world viewing conditions [Candy and Cormack 2022].

Recently, the sighting dominance experiments of Khan and Crawford [2001] were replicated in a VR setting [Prümmer et al. 2024], confirming that eye dominance varies dynamically during eye–hand coordination tasks with stimulus alignment. In contrast, our VR experiments target *acuity eye dominance* (AED) in purely visual tasks, focusing on asymmetric blur detection under binocular viewing. We study dominance variations across gaze directions, analogous to SD, and across retinal eccentricities via discrepant stimuli, analogous to SED. This focus on blur detection directly targets a key perceptual factor limiting the visibility of asymmetric distortions in stereoscopic imagery and naturally aligns with exploiting eye dominance in foveated rendering, as well as with related applications such as asymmetric stereoscopic video encoding [Meegan et al. 2001; Seuntiens et al. 2006] for VR/AR streaming and cloud gaming.

2.3 Foveation and Eye Dominance in Rendering

Retinal photoreceptors density decreases from the fovea toward the periphery [Curcio and Allen 1990], leading to reduced visual acuity and increased tolerance to image blur [Watson and Ahumada 2011]. This behavior is commonly modeled by extending the contrast sensitivity function to peripheral vision [Mantiuk et al. 2022; Peli et al. 1991], forming the basis of foveated rendering, where sampling density follows peripheral sensitivity falloff [Weier et al. 2017]. Building on this, numerous real-time gaze-driven methods modulate spatial image resolution [Guenter et al. 2012; Li et al. 2021; Patney et al. 2016; Ye et al. 2022], often incorporating local image statistics [Tursun et al. 2019] or visual saliency [Fan et al. 2024; Krajancich et al. 2023; Stengel et al. 2016]. To mitigate artifacts in heavily blurred peripheral regions, prior work synthesizes high-frequency noise [Tariq et al. 2022], reconstructs plausible detail from sparse, temporally accumulated samples using generative models [Kaplanyan et al. 2019], or compensates for losses in motion perception [Tariq and Didyk 2024]. Beyond these monocular considerations, binocular vision offers additional opportunities for perceptual optimization.

Eye dominance and reduced blur sensitivity of the non-dominant eye have therefore been exploited to further accelerate foveated rendering through more aggressive yet perceptually acceptable reductions in sampling density. Meng et al. [2020] introduce kernel foveated rendering (KFR), parameterizing peripheral blur with a single control value tuned to remain imperceptible in the non-dominant eye. Wang et al. [2025] demonstrate that this approach is overly conservative and improves performance by partitioning the field of view into multiple eccentricity-dependent zones for each eye. Prummer et al. [2025] were the first to postulate exploring dynamic eye dominance for foveated rendering. Motivated by this idea, we derive visual dominance maps that reveal spatially varying dominance as a function of retinal position relative to the fixation point, indicating that strategies assuming fixed dominance may be suboptimal.

3 Experiment 1: Dynamic Dominance in Fovea

In this section, we explore sighting dominance (Sec. 2.2) by studying how dynamic visual dominance influences monocular blur suppression across different fixation locations. Participants performed a blur discrimination task in which controlled amounts of blur were applied either binocularly or monocularly, while fixation was constrained to predefined locations within the headset's binocular region. Starting from standard binocular detection thresholds for foveal blur as a baseline, we analyze how these thresholds change under monocular blur in different fixation locations. Our results suggest that monocular blur detection thresholds are influenced by both the eye to which the blur is presented and gaze direction.

3.1 Experimental Setup

Hardware. We used a Varjo XR-4 headset with an integrated eye-tracker (200 Hz and 1° accuracy). A chin rest was employed to fix head position and stimuli were generated in screen-space, thereby avoiding head motion or jitter. The experiment procedure was implemented in Unity [1] and participants remained seated throughout the session. Rendering resolution was set to 51 PPD. Additional hardware details are provided in the S1 in the supplementary. To study visual dominance, we focus on binocularly visible visual field locations, i.e., the overlap region seen by both eyes. To ensure consistency across participants, this overlap region was kept constant by fixing the headset interpupillary distance (IPD) to 64 mm. As a result, the stereoscopic region considered in this experiment spans from −25° to 25° in the visual field, similar to previous works [Kergaßner et al. 2025]. This overlap region is illustrated in Fig. 2.

Stimuli. Following previous work in blur detection and discrimination [Watson and Ahumada 2011], the visual stimulus employed was a vertical sinusoidal pattern defining an edge between two luminance contrasts [Mather and Smith 2002]. This pattern provides a combination of vertical and horizontal cues, becoming closer to real scenes than single-dimensional edges. The stimulus pattern was generated at runtime using a GLSL shader following the sine wave equation along the vertical axis:

$$f(y) = 0.5 + A \cdot \sin(2\pi\omega \cdot y + \phi) \tag{1}$$

where A is the amplitude of the sinusoid, ω the spatial frequency in cycles per texture UV unit, and ϕ the phase. The values employed are:

[1] https://unity.com/

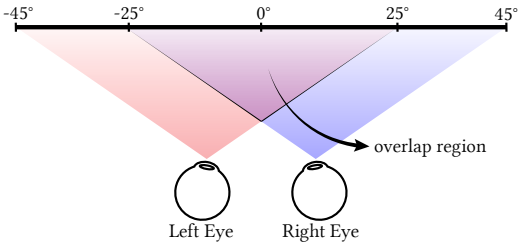

Fig. 2. Overlap region considered in our study where stereo viewing is available. Each eye individually sees a FOV of 70°, while the common central region is constrained to 50°, 25° from the center of the screen [Kergaßner et al. 2025]. Considering the monocular regions, the effective total FOV is 90°.

$A = 0.27$, $\omega = 2$ (cycles displayed), and $\phi = 0$. To achieve the desired stimuli contrast [Mather and Smith 2002], the two regions at each side of the border were assigned grayscale intensity values of 0.8 and 0.2, implemented as linear RGB triplets. The sinusoidal pattern (Fig. 3, top-right) was dichoptically shown in both eyes, while blur levels applied to each eye were independent. This was achieved by using a second post-processing GLSL shader that applied a stereoscopic Gaussian blur kernel. Details on how the Gaussian blur was applied are provided in S2 in supplementary. The visual stimulus subtended 5° of visual angle, covering the entire foveal region [Kergaßner et al. 2025]. To ensure that blur differences were visible, the stimulus texture resolution was set to 70 PPD. Texture downsampling to display resolution is done via mipmapped bilinear filtering, ensuring no aliasing effects impact the displayed blur level. Scene background was rendered with an intensity value of 0.5. Examples of blurred stimuli are shown in Fig. 3 (right).

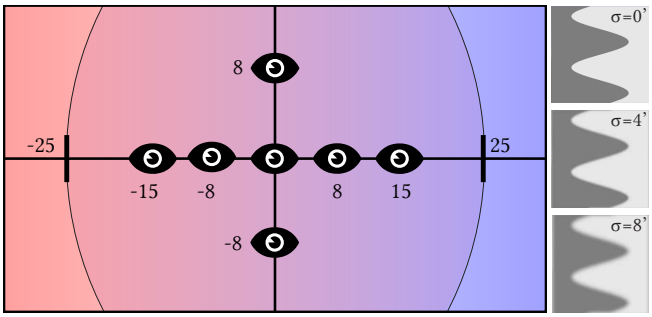

Fig. 3. *Left:* Illustration of the fixation locations considered in Experiment 1, together with the limits of the binocular region of the headset. *Right:* The visual stimulus employed, with blur levels of $\sigma = \{0', 4', 8'\}$.

Conditions. The main factor of this experiment is the *blur mode*, defined as $mode = \{Binocular, Left, Right\}$. In Binocular mode, both eye views receive the same blur level, while in Left and Right modes, blur is applied only to the left or right view, respectively. We consider three *blur levels* for all modes $\sigma = \{0.5', 1', 2'\}$. Since monocular blur is harder to detect, three additional blur levels $\sigma = \{4', 8', 16'\}$ are included for Left and Right modes. To test different gaze directions, we asked participants to fixate on the visual stimulus placed at different positions in the visual field, always within the stereoscopic region of the headset. We define fixation locations along the vertical and horizontal axes of the screen and denote them as (pos_{hor}, pos_{ver}), expressed in degrees of visual angle relative to the center of the screen, where positive values indicate rightward and upward offsets. We include the following *fixation locations* = $\{(0,0),\ (\pm 8,0),\ (\pm 15,0),\ (0,\pm 8)\}$. These locations follow typical fixation areas after visual saccades, whose amplitudes reach up to 15° without involving head motion [Bahill et al. 1975]. We employ a fully factorial design with 3 *modes* × 7 *fixation locations* × 3 or 6 *blur levels* (σ) = 105 conditions. Each condition was repeated six times, yielding 630 trials per participant.

Participants. Twelve participants took part in the study (8 male, 4 female, ages 20-26). All reported normal or corrected-to-normal vision and provided written consent to participate. The study protocol was approved by the Ethical Review Board of the Department of Computer Science at Saarland University. Only two of them were left-dominant, closely representing population distribution. From the participant pool, 83.3% reported having used VR equipment 5 times or less and only one participant never used it before. The full survey can be found in S6 in the supplementary.

Procedure. Participants performed a two-alternative forced-choice (2AFC) task comparing a blurred stimulus against an unblurred *Reference* ($\sigma = 0'$). In each trial, participants viewed two *Test Cases* in sequence and selected the one that appeared more similar to the Reference. One of the two Test Cases always matched the Reference exactly, while the other contained the blurred stimulus under evaluation. In this task, chance-level performance therefore corresponds to blur levels at which participants cannot consistently distinguish between the blurred and unblurred stimuli. The order of these two Test Cases was randomized on every trial. Each trial followed the same temporal sequence: Reference → Test Case 1 → Reference → Test Case 2, with the user being able to switch between them. A warning message asking the participant to make a decision was displayed after 10s or if the full sequence was repeated three times. Participants indicated their choice via button press. The system accepted responses only while participants maintained fixation on the stimulus, as verified by the eye-tracking data. We chose this temporal presentation to guarantee precise fixation without introducing spatial offsets that would engage peripheral vision. Each experimental session lasted approximately one and a half hours.

3.2 Results and Discussion

We compute success ratios based on the proportion of trials in which participants selected the unblurred Test Case, which is identical to the Reference. Higher success ratios indicate that blur is more reliably detected, reflecting stronger perceptual differences. For each condition, we aggregate responses across trials and participants, and use these ratios to estimate blur detection thresholds. We remove response-time outliers by excluding trials with response times

outside the 1st–99th percentile range. We then fit a logistic psychometric function (Eq. 2) defined over the logarithm of the blur level $\log_{10}(\sigma)$, parameterized by a location parameter α, slope β, and lapse rate λ. The guess rate is fixed to $\gamma = 0.5$ to match our experimental design. This function is commonly used in perceptual studies to model detection and discrimination performance, as it captures the characteristic sigmoidal relationship between stimulus strength and response probability while allowing for chance-level performance in forced-choice tasks.

$$P(x) = \gamma + (1 - \gamma - \lambda)\,\frac{1}{1 + \exp\left(-\frac{\log_{10}(x) - \alpha}{\beta}\right)}. \tag{2}$$

Since fitting individual curves would be unstable due to limited data, we first pool responses across observers [Bernal-Berdun et al. 2025; Patney et al. 2016; Wang and Kristensson 2026; Wolski et al. 2022]. To verify that pooled fits reflect consistent behaviour, we assessed the monotonic relationship between blur level and detection probability using Spearman's ρ. In our results, 89% of participant–condition cases exhibited $\rho > 0$, 71% exceeded $\rho > 0.5$, and 11% showed $\rho < 0$, supporting the pooled fits as a stable population-level estimate. The fitted curves for horizontal (avg. RMSE: 0.034 and R^2: 0.913) and vertical (avg. RMSE: 0.031 and R^2: 0.932) fixation locations are shown in Fig. 10 and Fig. 11, respectively. As expected, all curves originate at the chance level (50%), consistent with the 2AFC task. We derive detection thresholds at the 75% performance level by obtaining the blur value at which each fitted curve intersects the 75% point (green dotted line). The detection thresholds are shown in Fig. 4 and a visualization of raw data is provided in the Supplementary S3.

As shown in the results, blur detection thresholds in the Binocular condition remain below 1′, consistent with previous findings in blur detection studies [Watson and Ahumada 2011]. These thresholds do not vary with gaze direction, indicating that foveal acuity remains stable across the stereoscopic region of the field of view considered. This binocular condition, therefore, provides a stable baseline against which monocular effects can be interpreted.

When blur is applied to a single eye, detection thresholds increase relative to the binocular baseline. Interestingly, these monocular conditions reveal a dynamic visual dominance with a clear dependence on gaze direction. As shown in Fig. 4 (top), blur detection thresholds for the left eye increase when participants fixate toward the right side of the screen, and vice versa. This suggests that blur tolerance increases for blurry inputs on the eye that does not fully cover the corresponding side of the field of view (e.g., left eye on the right side). In other words, dynamic visual dominance modulates monocular blur suppression as a function of gaze direction.

In our data, the transition between left and right eye dominance occurs at approximately 3–4° to the right of the screen center. Although most participants exhibit right-eye dominance overall, we observe higher blur tolerance in the Right condition when fixation is centered. This transition point differs slightly from prior reports in hand–eye alignment tasks, which place the dominance switch around 5° to the left [Prümmer et al. 2024], suggesting that dominance transitions may depend on task demands and stimulus properties. Despite this shift, our thresholds are consistent across

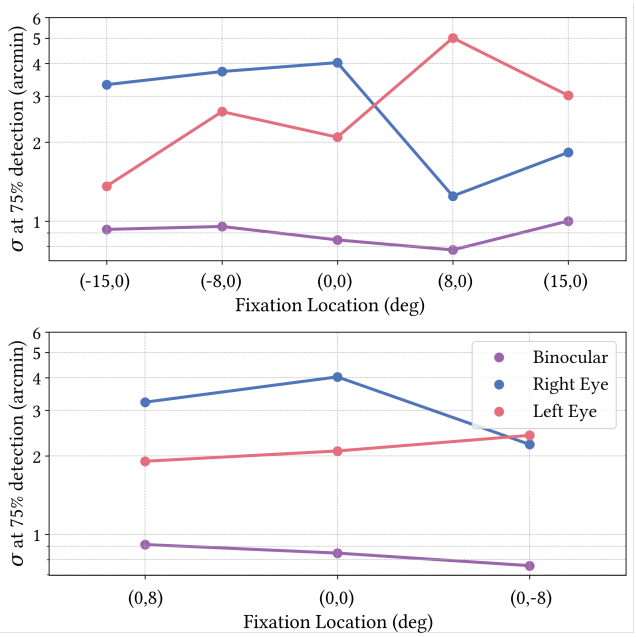

Fig. 4. Blur Detection Thresholds for horizontal (top) and vertical (bottom) fixation locations (Experiment 1). The X-axis shows locations from the screen center denoted as (pos_{hor}, pos_{ver}), expressed in degrees of visual angle. For horizontal locations, a higher threshold is measured for the left eye on the right side of the screen (right-eye dominance). Conversely, left-eye dominance is observed on the left side. Unlike horizontal locations, vertical locations do not flip visual dominance significantly. Instead, eye dominance remains the same as in the central location. Regarding binocular blur, detection thresholds do not strongly depend on the gaze direction.

conditions, with thresholds below 1′ for binocular blur [Watson and Ahumada 2011]; thresholds between 1′ and 3′ for the dominant eye; and larger thresholds between 3′ and 5′ for the non-dominant eye.

For vertical fixation locations, we hypothesized no systematic modulation of visual dominance as both eyes symmetrically cover the vertical extent of the visual field. The results in Fig. 4 (bottom) qualitatively support this expectation, showing little apparent change in blur detection thresholds. Although the $(0, -8)$ case shows no clear dominance, further exploration is needed to confirm this behaviour.

In summary, we show for the first time that monocular blur detection thresholds are not only elevated relative to binocular viewing, but are also systematically modulated by gaze direction and by which eye is blurred.

4 Experiment 2: Dynamic Dominance in Periphery

After studying how foveal visual dominance varies with gaze direction, we now extend our analysis to peripheral vision. The goal now is to determine whether similar dominance shifts occur for stimuli presented at different retinal eccentricities relative to the current gaze direction, as in sensory eye dominance experiments (Sec. 2.2). Participants performed a blur discrimination task in which blur was always present but monocularly applied to either the left

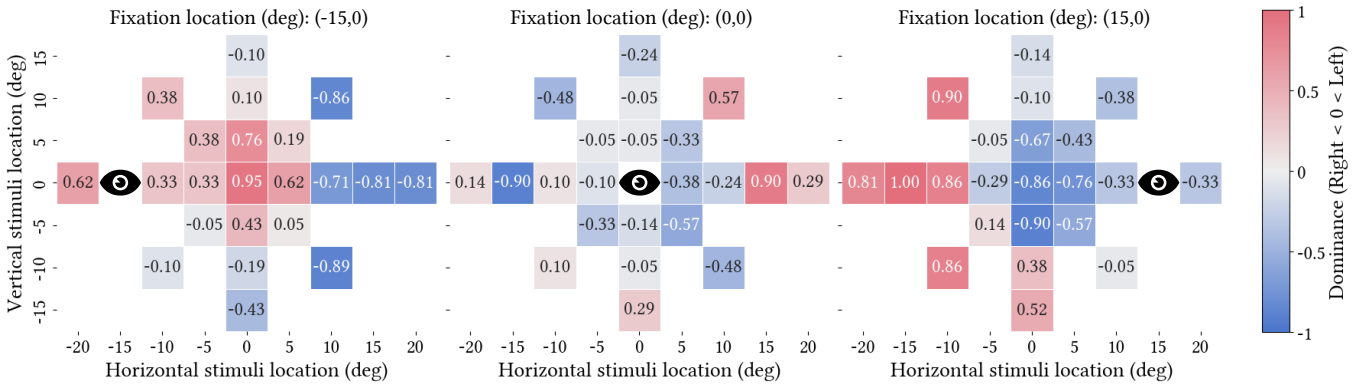

Fig. 5. Results obtained in Experiment 2. Different fixation locations are represented: *left side* fixation at (0,-15); *center* fixation at (0,0); *right side* fixation at (0,15). Ratios show monocular dominance by the means of the preferred input being blurred. Values close to 1 show left eye dominance (right eye blur preferred), while values close to -1 show right eye dominance. Axes represent locations in screen space, expressed in degrees of visual angle.

or right eye. While participants fixated at predefined locations, we presented the stimulus at different peripheral positions within the stereoscopic region, and asked them to select the presentation that appeared more similar to the unblurred Reference. This design allows us to characterize peripheral visual dominance by comparing preference between left- and right-eye blur as a function of both gaze direction and stimulus eccentricity. We use the same hardware and stimuli as previously reported (Sec. 3.1).

Conditions. Following the same notation (pos_{hor}, pos_{ver}), we define three fixation locations along the horizontal axis such that *fixation location* = $\{(-15, 0), (0, 0), (15, 0)\}$, expressed in degrees of visual angle relative to the screen center. To study visual dominance in the periphery, stimulus locations are also presented at discrete locations relative to the screen center, ensuring stereoscopic viewing. We define the stimulus locations as *stimulus location* = $\{(0, 0), (\pm5, 0), (\pm10, 0), (\pm15, 0), (\pm20, 0), (0, \pm5), (0, \pm10), (0, \pm15), (\pm5, \pm5), (\pm10, \pm10)\}$, where coordinates denote horizontal and vertical offsets in degrees of visual angle. All stimulus locations considered are displayed in Fig. 6. We employ a fully factorial design with 3 *fixation locations* × 22 *stimulus locations* = 66 conditions. Each condition is repeated six times, yielding 396 trials per participant.

Procedure. The visual stimulus is as described in Sec. 3.1, and we follow a similar sequential presentation. In this experiment, both stimulus presentations (Test Case 1 and Test Case 2) contain blur, but each presentation shows the stimulus blurred in either the *Left* or *Right* view. The participants' task was to select the Test Case that appeared more similar to the unblurred *Reference*. To ensure that monocular blur remains detectable in the periphery, we set the applied blur well above the foveation-dependent detection threshold. We define the applied blur as: $\sigma_{applied}(E) = \sigma_{foveation}(E) \cdot 1.5$; where: $\sigma_{foveation}(E) = 0.3 \cdot Eccentricity(^\circ)$. Such a blur increase ratio follows established foveated rendering guidelines for peripheral blur [Mantiuk et al. 2022; Patney et al. 2016]. To guarantee that judgments rely on peripheral perception, participants had to fixate on a cross. Whenever gaze deviated from the intended fixation location, the stimulus disappeared and responses were not accepted.

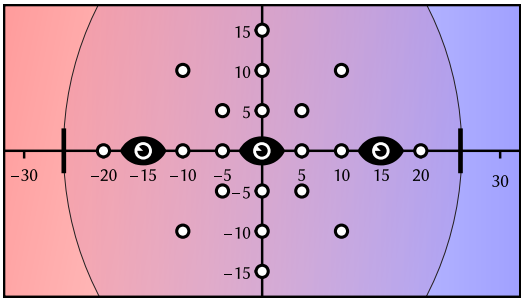

Fig. 6. Stimuli and fixation locations considered in Experiment 2. Three fixation locations are considered, being at (0,0), (15,0) and (-15,0). For each fixation location, stimuli locations covering the headset overlapping region are also represented by dots.

Participants. A total of 7 participants performed the study (4 male, 3 female, ages 21-27). All of them reported normal or corrected-to-normal vision and provided written consent to participate. In this case, four participants reported having used VR equipment 5 times or less, and only one participant never used it before.

4.1 Results and Discussion

For each condition, we compute the proportion of trials in which participants selected the Right (right eye blurred) or Left (left eye blurred) condition as being more similar to the unblurred Reference. These ratios reflect relative monocular dominance: positive values indicate a preference for right-eye blur, negative values indicate a preference for left-eye blur, and larger magnitudes correspond to greater blur tolerance in the preferred eye. The resulting dominance ratios are shown in Fig. 5, grouped by fixation location.

As shown in these results, the dominant view shifts systematically across the peripheral locations within the overlapping region. Consistency across participants is quantified by correlating each participant's response map with the leave-one-out group mean, obtaining strong agreement (mean Pearson $r = 0.71, SD = 0.11$;

mean Spearman $\rho = 0.69$). This suggests that the spatial dominance pattern is largely shared across observers, despite local variability.

When the fixation location is at $(0, 0)$, stronger dominance shifts appear around eccentricities of ±15°, corresponding to the blind spots of the left and right eyes, respectively. At peripheral locations closer to the fixation, no strong dominance toward either eye is observed, although a slight preference for left-eye blur emerges, consistent with the predominance of right-eye dominance across participants. With fixation location shifted to the left $(-15, 0)$, left-eye dominance appears for small eccentricities around the fovea until the right-eye blind spot at +15° from fixation. Beyond this point, dominance switches to the right eye and persists toward the periphery, up to the maximum eccentricity tested. A symmetric pattern emerges when fixation shifts to the right $(15, 0)$, with right-eye dominance near the fovea and a switch to left-eye dominance beyond the left-eye blind spot. These dominance reversals in peripheral regions starting at $E = 20°$ reflect the naso-temporal asymmetry in binocular vision, where input from the nasal retina dominates over that from the temporal retina at large eccentricities [Fahle 1987; Fahle and Schmid 1988]. The blind spots around ±15° act as transition points that trigger local dominance switches, producing a continuous and coherent binocular percept across the visual field.

Retinal Dominance Map. To build a unified Retinal Dominance Map, we merged data from all three fixation conditions. As shown in Fig. 5, visual dominance shifts consistently, with blind-spot transitions occurring at ±15° relative to the fovea regardless of gaze direction. This suggests that, within the tested stereoscopic range, peripheral dominance is primarily driven by retinal eccentricity of the stimulus with respect to the fixation location. Based on this observation, we integrate the data across fixation conditions by transforming stimulus positions to fovea-centered coordinates $(\Delta x, \Delta y) = (s_x - f_x, s_y - f_y)$, pooling samples with identical retinal offsets. For those relative coordinates sampled by multiple gaze locations, agreement is lower near the fovea ($E \leq 10°$: mean $SD = 0.45$) than in the periphery ($10 < E < 20$: mean $SD = 0.15$), as can be observed in Fig. 5. Therefore, since visual dominance in relative locations close enough to the fovea is affected by gaze direction, such locations are excluded from the peripheral map. For the remaining locations, cross-fovea consistency is tested via a neighbor-based prediction from nearby positions measured under other fixation conditions. Observed and predicted dominance values strongly correlate (Pearson $r = 0.70, p < 0.001$), indicating coherent spatial structure, thus supporting the merging and interpolation. The resulting peripheral dominance map is shown in Fig. 7 and used in our tested application (Sec. 5.1).

5 Application Cases

We propose potential applications for the dynamic visual dominance phenomenon. We use our findings to establish a visual dominance map in the continuous domain to guide gaze-contingent rendering while accounting for dominance shifts. In addition, we estimate computing savings by developing a desktop-based Variable Rate Shading (VRS) prototype and devising a combined map that relates visual dominance to both fixation location and stimulus eccentricity.

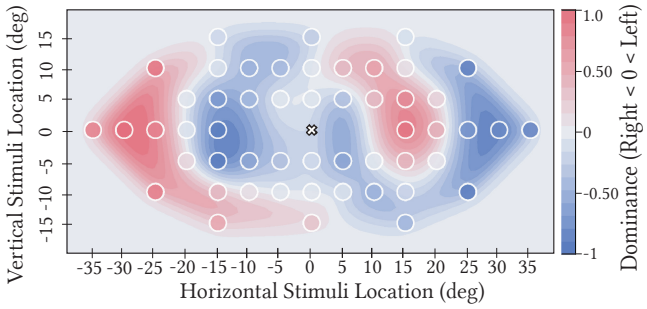

Fig. 7. Peripheral dominance map obtained by interpolating the data obtained from the eccentricity values considered in Experiment 2 (Fig. 5). Stimulus locations are relative to the fovea and expressed in degrees of visual angle. Small horizontal eccentricities (E=±5°, ±10°) are not combined, as their proximity to the fovea makes gaze angle influence visual dominance.

5.1 Guiding Visual Dominance-Contingent Rendering

Our dominance map from Sec. 4 can be used to add additional blur levels to the peripheral non-dominant regions of each eye. As in gaze-contingent approaches, we focus on peripheral dominance potential while the foveal region is unmodified. To do so, we first calculate dense peripheral dominance values in a 2D spatial grid using cubic interpolation following a Clough-Tocher scheme [Alfeld 1984; Farin 1986]. Such a 2D spatial grid allows us to estimate ocular dominance, labeled as $d\left(s_{x,y}\right)$, for any stimulus location within the stereoscopic field (Fig. 7), where $d \in [-1, 1]$ indicates the visual dominance level. To perform the interpolation, we leverage our experiment-acquired dominance ratios (Sec. 4) as sparse input conditions $(d\left(s^i_{x,y}\right))$. The resulting interpolated map allows continuous peripheral dominance transition effects driven by retinal eccentricity. By sampling the map in real time, dynamic dominance can be considered through higher foveation blur in the non-dominant regions of each eye. We adapt the rendering pipeline to apply our dominance map as gaze-contingent foveation blur levels. To perceptually evaluate our method, we use post-processing shaders in Unity. Following the experimental procedure of previous sections, we use standard foveated rendering as baseline, where $\sigma_{left} = \sigma_{right} = \sigma_{foveation}$ (Sec. 4). We implemented static dominance rendering, where blur increments are statically applied in the non-dominant input (left eye) [Wang et al. 2023, 2025], as an alternative to our method. Specifically, we apply: $\sigma_{left} = 1.5 \cdot \sigma_{foveation}; \sigma_{right} = \sigma_{foveation}$. The 1.5 multiplication factor of the non-dominant eye refers to previous work [Meng et al. 2020]. For our method, we derive eye-dependent blur intensity maps from the peripheral dominance map $d(s_{x,y})$ (Fig. 7). The left-eye blur map $b_l(s_{x,y})$ is obtained by reparameterizing the negative dominance range $[-1, 0]$ to $[1, 0]$, such that higher values indicate increased blur applied to the left eye in regions dominated by the right eye. Conversely, the right-eye blur map $b_r(s_{x,y})$ maintains the positive dominance range $[0, 1]$, assigning higher values to left-eye dominated regions so extra blur is applied in the right view. Thus, $b_{l,r}(s_{x,y}) \in [0, 1]$. Blur kernel $\sigma_{l,r} \in [1, 3]$ is then set as follows:

$$\sigma_{l,r}\left(s_{x,y}\right) = 2 \cdot \min\left(1, \max\left(2 \cdot b_{l,r}\left(s_{x,y}\right) - 1, 0\right)\right) + 1. \quad (3)$$

This transformation is displayed in S4 in the supplementary. Therefore, the stereoscopically applied blur is: $\sigma_{applied} = \sigma_{l,r}\left(s_{x,y}\right) \cdot \sigma_{foveation}$. Non-dominant regions are dynamically sampled in real-time from the peripheral dominance map based on the eye-tracked gaze. A representation of how these regions are sampled in screen space can also be seen in Supplementary S4.

As a result, the non-dominance factor ranges in the [1,3] interval, where 1 corresponds to the dominant regions and 3 to the strongest non-dominant regions. We limit this factor to 3 to test the capabilities of our method by doubling the factor considered in the static dominance approach, and to not apply an excessive blur amount that may cause discomfort. Please refer to Sec. 6 for further discussion.

In a perceptual study, we compare our method and the static dominance approach with standard foveated rendering as *Reference*. Eleven participants (9 male, 2 female, ages 21–35) took part in the study. The task was to choose which method is perceived closer to the *Reference* in terms of blur and image resolution. In every scene, participants were instructed to fixate on some specific region and focus on: comparing the lion shields (*Sponza*); the bears in the background (*Nature*); and the back of the seated man (*2D Image*). Nevertheless, free viewing was allowed. Regions outside the overlapping region were blacked out to ensure attention control [Kergaßner et al. 2025]. Results are shown in Fig. 8.

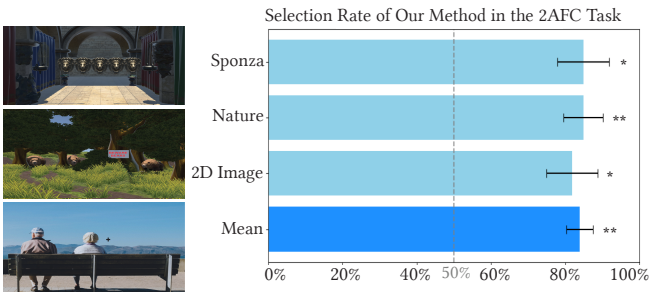

Fig. 8. Results obtained in our application case. Rates show a preference for choosing our dynamic dominance gaze contingent method over static dominance in the three scenarios considered. Error bars show standard error of the mean (SEM) and stars indicate significance ($^{*} < .005$,$^{**} < .0005$) compared to chance level (50%).

Our method is significantly preferred over the static eye dominance approach, with an 83.8% mean selection rate. A t-test analysis confirmed that all scenes: *Sponza* ($t = 5.043$, $p < .005$); *Nature* ($t = 6.640$, $p < .0005$); and *2D Image* ($t = 4.605$, $p < .005$), show selection rates significantly different from chance level.

Additionally, five of those participants repeated the study with full-resolution rendering as *Reference*. Even in such a case, our method remains preferred over the static dominance approach ($rate = 0.844, SEM = 0.055, t = 6.254, p < .001$). Since our aim is to show that visual dominance behaves dynamically, no other foveation methods that consider additional variables (e.g. contrast or saliency) are compared with our technique.

5.2 Computational Savings Estimation in a VRS Prototype

A desktop-based variable rate shading (VRS) prototype has been implemented by using the Unity VRS API, which allows us to estimate the computational benefits of using our peripheral dominance map. Display resolution is set at 2550×2550, matching the stereo region of the headset. We encode the dominance map as a shading rate image, assigning corresponding shading rates per peripheral location. By targeting the complete non-dominant view, we compare applying a 4×4 shading rate in the strongest dominance regions with a uniform 1×1 shading rate as a baseline. When more stereo regions are monocularly dominated (e.g., Fig. 5, right), we obtain around 15% rendering savings. Similar gains are found with 4K or 8K resolution since the mask is constant in screen space. While gains depend on gaze direction and monocularly dominated regions within stereoscopic regions, larger savings are expected in more complex shading scenes, amplifying VRS benefits [Jindal et al. 2021]. Further implementation details are provided in S5 in the supplementary.

5.3 Combined Dominance Map

While our application primarily exploits peripheral dominance effects for visual dominance-contingent rendering (Sec. 5.1), a more complete dominance representation would be beneficial for a broader range of rendering strategies. Applications such as eye-asymmetric rendering require an understanding of how dominance varies across the visual field, from the fovea to the periphery, in order to adapt visual quality continuously as gaze and stimulus position change. Our foveal (Sec. 3) and peripheral (Sec. 4) findings provide complementary evidence toward this goal as both experiments show consistent dominance trends. Thus, Fig. 9 shows a conceptual dominance representation by relating the fovea-stimuli horizontal offset.

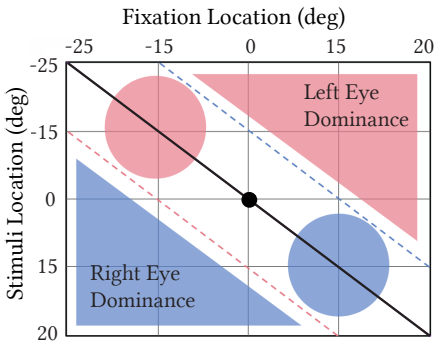

Fig. 9. Dominance representation along the horizontal dimension for different combinations of fixation and stimuli locations. Red and blue colors show left and right eye dominance, respectively. The diagonal line shows fixating at the stimuli and axes are expressed in degrees of visual angle from the screen center, while geometric shapes displayed are representative.

6 Conclusion and Future Work

In this work, we characterize dynamic visual dominance in stereoscopic vision, focusing on how asymmetric interocular blur is tolerated across the visual field.

Through two complementary psychophysical experiments, we show that blur binocularly applied within the foveal region is detected more readily than blur applied monocularly. We further show that blur detection thresholds vary with gaze direction (fovea) and

retinal eccentricity (periphery), revealing dynamic visual dominance even in basic visual acuity tasks. Beyond characterizing this phenomenon, we show how peripheral dominance can be leveraged in an application case for dominance-contingent rendering, where increased blur is selectively applied to the non-dominant eye. Despite the scope of our findings, several limitations remain and motivate future research directions.

To begin with, while non-dominant peripheral regions tolerate substantially higher blur than dominant ones, the upper bound of acceptable monocular blur and its interaction with binocular rivalry onsets (see [Fahle 1982]) were not explored in this work. Characterizing this trade-off could further extend perceptually guided computation savings.

Furthermore, in our current application, dominance transition zones are treated conservatively to ensure spatiotemporal stability and avoid visual artifacts. Future work could study the temporal dynamics of these transitions and explore strategies to safely exploit them. In addition, integrating the proposed application into a full foveated rendering or ray-tracing pipeline would allow a precise quantification of performance gains.

Finally, visual dominance may extend to other forms of dynamic visual effects. For instance, prior work has explored peripheral color modulations for display power savings [Duinkharjav et al. 2022], exploited change blindness effects [Groth et al. 2023], and showed changes in speed perception [Peng et al. 2025; Scholz et al. 2024]. Whether similar dominance-driven tolerance exists for those attributes remains an interesting direction for future research. In this context, our preliminary exploration of peripheral dominance in color space through stereoscopic color variations suggests that dynamic dominance may also be leveraged along these dimensions.

For the first time, our work shows that visual dominance in stereoscopic vision dynamically modulates monocular blur tolerance across both foveal and peripheral vision. To foster future research, our collected anonymized data is publicly available at https://dynamicvisualdominance.mpi-inf.mpg.de.

Acknowledgments

This work has received funding from the European Union (ERC grant number 101220555, PROXIE). Views and opinions expressed are however those of the author(s) only and do not necessarily reflect those of the European Union or the European Research Council Executive Agency. Neither the European Union nor the granting authority can be held responsible for them. This project has also received funding from grant PID2022-141539NB-I00, funded by MICIU/AEI/10.13039/501100011033 and by ERDF, EU. We also gratefully acknowledge the support of the Saarland/Intel Joint Program on the Future of Graphics and Media, and thank study subjects for their participation and reviewers for their suggestions.

References

Peter Alfeld. 1984. A trivariate clough—tocher scheme for tetrahedral data. *Computer Aided Geometric Design* 1, 2 (1984), 169–181.

Derek H Arnold, Philip M Grove, and Thomas SA Wallis. 2007. Staying focused: A functional account of perceptual suppression during binocular rivalry. *Journal of Vision* 7, 7 (2007), 7–7.

A Terry Bahill, Deborah Adler, and Lawrence Stark. 1975. Most naturally occurring human saccades have magnitudes of 15 degrees or less. *Investigative Ophthalmology & Visual Science* 14, 6 (1975), 468–469.

Martin S. Banks, Tandra Ghose, and James M. Hillis. 2004. Relative Image Size, Not Eye Position, Determines Eye Dominance Switches. *Vision Research* 44, 3 (2004), 229–234. doi:10.1016/j.visres.2003.09.029

Edurne Bernal-Berdun, Mateo Vallejo, Qi Sun, Ana Serrano, and Diego Gutierrez. 2025. Audiovisual Disparities in VR: Impact on Spatial Perception. In *2025 IEEE International Symposium on Mixed and Augmented Reality (ISMAR)*. IEEE, 1–8.

T Rowan Candy and Lawrence K Cormack. 2022. Recent understanding of binocular vision in the natural environment with clinical implications. *Progress in retinal and eye research* 88 (2022), 101014.

Jianhua Cang, Jieming Fu, and Seiji Tanabe. 2023. Neural circuits for binocular vision: Ocular dominance, interocular matching, and disparity selectivity. *Frontiers in Neural Circuits* 17 (2023), 1084027.

David P Carey and Claire V Hutchinson. 2013. Looking at eye dominance from a different angle: is sighting strength related to hand preference? *Cortex* 49, 9 (2013), 2542–2552.

Romain Chaumillon, Nadia Alahyane, Patrice Senot, Judith Vergne, Christelle Lemoine-Lardennois, Jean Blouin, Karine Doré-Mazars, Alain Guillaume, and Dorine Vergilino-Perez. 2017. Asymmetry in visual information processing depends on the strength of eye dominance. *Neuropsychologia* 96 (2017), 129–136.

B. D. Chaurasia and B. B. Mathur. 1976. Eyedness. *Acta Anatomica* 96, 2 (1976), 301–305.

Christine A. Curcio and Kimberly A. Allen. 1990. Topography of Ganglion Cells in Human Retina. *The Journal of Comparative Neurology* 300, 1 (1990), 5–25.

Budmonde Duinkharjav, Kenneth Chen, Abhishek Tyagi, Jiayi He, Yuhao Zhu, and Qi Sun. 2022. Color-Perception-Guided Display Power Reduction for Virtual Reality. *ACM Trans. Graph.* 41, 6, Article 210 (Nov. 2022), 16 pages. doi:10.1145/3550454.3555473

M Fahle. 1982. Binocular rivalry: Suppression depends on orientation and spatial frequency. *Vision research* 22, 7 (1982), 787–800.

Manfred Fahle. 1987. Naso-temporal asymmetry of binocular inhibition. *Investigative ophthalmology & visual science* 28, 6 (1987), 1016–1017.

M Fahle and M Schmid. 1988. Naso-temporal asymmetry of visual perception and of the visual cortex. *Vision research* 28, 2 (1988), 293–300.

Runze Fan, Xuehuai Shi, Kangyu Wang, Qixiang Ma, and Lili Wang. 2024. Scene-aware foveated rendering. *IEEE Transactions on Visualization and Computer Graphics* (2024).

Gerald Farin. 1986. Triangular bernstein-bézier patches. *Computer Aided Geometric Design* 3, 2 (1986), 83–127.

Mark A Georgeson and Stuart A Wallis. 2014. Binocular fusion, suppression and diplopia for blurred edges. *Ophthalmic and Physiological Optics* 34, 2 (2014), 163–185.

Colin Groth, Timon Scholz, Susana Castillo, Jan-Philipp Tauscher, and Marcus Magnor. 2023. Instant Hand Redirection in Virtual Reality Through Electrical Muscle Stimulation-Triggered Eye Blinks. In *ACM Symposium on Virtual Reality Software and Technology (VRST)*. 1–11. doi:10.1145/3611659.3615717

Brian Guenter, Mark Finch, Steven Drucker, Desney Tan, and John Snyder. 2012. Foveated 3D Graphics. *ACM Transactions on Graphics* 31, 6 (2012). Proceedings of SIGGRAPH Asia.

David M Hoffman and Martin S Banks. 2010. Focus information is used to interpret binocular images. *Journal of vision* 10, 5 (2010), 13–13.

Daniel Jiménez-Navarro, Colin Groth, Xi Peng, Jorge Pina, Qi Sun, Praneeth Chakravarthula, Karol Myszkowski, Hans-Peter Seidel, and Ana Serrano. 2026. Overdriving Visual Depth Perception via Sound Modulation in VR. *IEEE Transactions on Visualization and Computer Graphics* (2026).

Akshay Jindal, Krzysztof Wolski, Karol Myszkowski, and Rafał K Mantiuk. 2021. Perceptual model for adaptive local shading and refresh rate. *ACM Transactions on Graphics (TOG)* 40, 6 (2021), 1–18.

Anton S. Kaplanyan, Anton Sochenov, Thomas Leimkühler, Mikhail Okunev, Todd Goodall, and Gizem Rufo. 2019. DeepFovea: neural reconstruction for foveated rendering and video compression using learned statistics of natural videos. *ACM Trans. Graph.* 38, 6, Article 212 (2019).

Sophie Kergaßner, Taimoor Tariq, and Piotr Didyk. 2025. Towards Understanding Depth Perception in Foveated Rendering. In *Proceedings of the Special Interest Group on Computer Graphics and Interactive Techniques Conference Conference Papers*. 1–9.

Aarlenne Z Khan and J Douglas Crawford. 2001. Ocular dominance reverses as a function of horizontal gaze angle. *Vision research* 41, 14 (2001), 1743–1748.

Brooke Krajancich, Petr Kellnhofer, and Gordon Wetzstein. 2023. Towards attention–aware foveated rendering. *ACM Transactions on Graphics (TOG)* 42, 4 (2023), 1–10.

David Li, Ruofei Du, Adharsh Babu, Camelia D Brumar, and Amitabh Varshney. 2021. A log-rectilinear transformation for foveated 360-degree video streaming. *IEEE Transactions on Visualization and Computer Graphics* 27, 5 (2021), 2638–2647.

Rafał K Mantiuk, Maliha Ashraf, and Alexandre Chapiro. 2022. stelaCSF: a unified model of contrast sensitivity as the function of spatio-temporal frequency, eccentricity, luminance and area. *ACM Transactions on Graphics (TOG)* 41, 4 (2022), 1–16.

George Mather and David RR Smith. 2002. Blur discrimination and its relation to blur-mediated depth perception. *Perception* 31, 10 (2002), 1211–1219.

D. V. Meegan, L. B. Stelmach, and W. J. Tam. 2001. Unequal Weighting of Monocular Inputs in Binocular Combination: Implications for the Compression of Stereoscopic

Imagery. *Experimental Psychology* 7, 2 (2001), 143–153.
Xiaoxu Meng, Ruofei Du, and Amitabh Varshney. 2020. Eye-dominance-guided foveated rendering. *IEEE Transactions on Visualization and Computer Graphics* 26, 5 (2020), 1972–1980.
Chris LE Paffen. 2025. Variations in sensory eye dominance along the horizontal meridian. *Journal of Vision* 25, 8 (2025), 1–1.
Anjul Patney, Marco Salvi, Joohwan Kim, Anton Kaplanyan, Chris Wyman, Nir Benty, David Luebke, and Aaron Lefohn. 2016. Towards foveated rendering for gaze-tracked virtual reality. *ACM Transactions On Graphics (TOG)* 35, 6 (2016), 1–12.
Eli Peli, Jian Yang, and Robert B. Goldstein. 1991. Image Invariance with Changes in Size: The Role of Peripheral Contrast Thresholds. *Journal of the Optical Society of America A* 8, 11 (Nov. 1991), 1762–1774.
Xi Peng, Colin Groth, Daniel Jimenez Navarro, Zihao Zou, Yan Zhu, Ana Serrano, Karol Myszkowski, Qi Sun, and Praneeth Chakravarthula. 2025. Why Slow Feels Fast and Fast Feels Slow: Evaluating and Predicting Speed Misperception. In *2025 IEEE International Symposium on Mixed and Augmented Reality (ISMAR)*. IEEE, 1075–1084.
Fabian Prümmer, Ludwig Sidenmark, and Hans Gellersen. 2024. Dynamics of Eye Dominance Behavior in Virtual Reality. *Journal of Eye Movement Research* 17, 3 (2024), 2.
Franziska Prummer, Florian Weidner, and Hans Gellersen. 2025. All But Static: Exploring Dynamic Eye Dominance for Foveated Rendering. In *2025 IEEE Conference on Virtual Reality and 3D User Interfaces Abstracts and Workshops (VRW)*. IEEE, 376–380.
J. Quartley and A. Y. Firth. 2004. Binocular Sighting Ocular Dominance Changes with Different Angles of Horizontal Gaze. *Binocular Vision & Strabismus Quarterly* 19, 1 (2004), 25–30.
Timon Scholz, Colin Groth, Susana Castillo, Martin Eisemann, and Marcus Magnor. 2024. Measuring Velocity Perception Regarding Stimulus Eccentricity. In *ACM Symposium on Applied Perception (SAP)*. ACM, 1–9.
Pieter Seuntiens, Lamberto Meesters, and Wijnand IJsselsteijn. 2006. Perceived Quality of Compressed Stereoscopic Images: Effect of Symmetric and Asymmetric JPEG Coding and Camera Separation. *ACM Transactions on Applied Perception* 3, 2 (April 2006), 96–109.
George Sperling. 1970. Binocular vision: A physical and a neural theory. *The American Journal of Psychology* (1970), 461–534.
James Stanley, Owen Carter, and Jason Forte. 2011. Color and Luminance Influence, but Cannot Explain, Binocular Rivalry Onset Bias. *PLoS ONE* 6, 5 (2011), e18978.
James Stanley, Jason D. Forte, and Owen Carter. 2019. Rivalry Onset In and Around the Fovea: The Role of Visual Field Location and Eye Dominance on Perceptual Dominance Bias. *Vision* 3, 4 (2019), 51. doi:10.3390/vision3040051
Michael Stengel, Steve Grogorick, Martin Eisemann, and Marcus Magnor. 2016. Adaptive image-space sampling for gaze-contingent real-time rendering. In *Computer graphics forum*, Vol. 35. Wiley Online Library, 129–139.
David Stidwill and Robert Fletcher. 2017. *Normal binocular vision: Theory, investigation and practical aspects*. John Wiley & Sons.
Taimoor Tariq and Piotr Didyk. 2024. Towards motion metamers for foveated rendering. *ACM Transactions on Graphics (TOG)* 43, 4 (2024), 1–10.
Taimoor Tariq, Cara Tursun, and Piotr Didyk. 2022. Noise-based enhancement for foveated rendering. *ACM Transactions on Graphics (TOG)* 41, 4 (2022), 1–14.
Okan Tarhan Tursun, Elena Arabadzhiyska-Koleva, Marek Wernikowski, Radosław Mantiuk, Hans-Peter Seidel, Karol Myszkowski, and Piotr Didyk. 2019. Luminance-contrast-aware foveated rendering. *ACM Trans. Graph.* 38, 4, Article 98 (2019).
Qisong Wang and Per Ola Kristensson. 2026. Stiffness Discrimination Thresholds of Force-Feedback Gloves for Volumetric Data Exploration in Virtual Reality. *IEEE Transactions on Visualization and Computer Graphics* (2026).
Zhimin Wang, Xiangyuan Gu, and Feng Lu. 2023. Deamp: Dominant-eye-aware foveated rendering with multi-parameter optimization. In *2023 IEEE International Symposium on Mixed and Augmented Reality (ISMAR)*. IEEE, 632–641.
Z. Wang, X. Gu, and F. Lu. 2025. Dominant-Eye-Aware Asymmetric Foveated Rendering for Virtual Reality. *IEEE Transactions on Visualization and Computer Graphics* 31, 10 (2025), 9225–9236. doi:10.1109/TVCG.2025.3593899
Andrew B. Watson and Albert J. Ahumada. 2011. Blur Clarified: A Review and Synthesis of Blur Discrimination. *Journal of Vision* 11, 5 (2011), 10.
Martin Weier, Michael Stengel, Thorsten Roth, Piotr Didyk, Elmar Eisemann, Martin Eisemann, Steve Grogorick, André Hinkenjann, Ernst Kruijff, Marcus Magnor, Karol Myszkowski, and Philipp Slusallek. 2017. Perception-Driven Accelerated Rendering. *Computer Graphics Forum* 36, 2 (2017), 611–643.
Krzysztof Wolski, Laura Trutoiu, Zhao Dong, Zhengyang Shen, Kevin Mackenzie, and Alexandre Chapiro. 2022. Geo-metric: A perceptual dataset of distortions on faces. *ACM Transactions on Graphics (TOG)* 41, 6 (2022), 1–13.
Jiannan Ye, Anqi Xie, Susmija Jabbireddy, Yunchuan Li, Xubo Yang, and Xiaoxu Meng. 2022. Rectangular mapping-based foveated rendering. In *2022 IEEE Conference on Virtual Reality and 3D User Interfaces (VR)*. IEEE, 756–764.

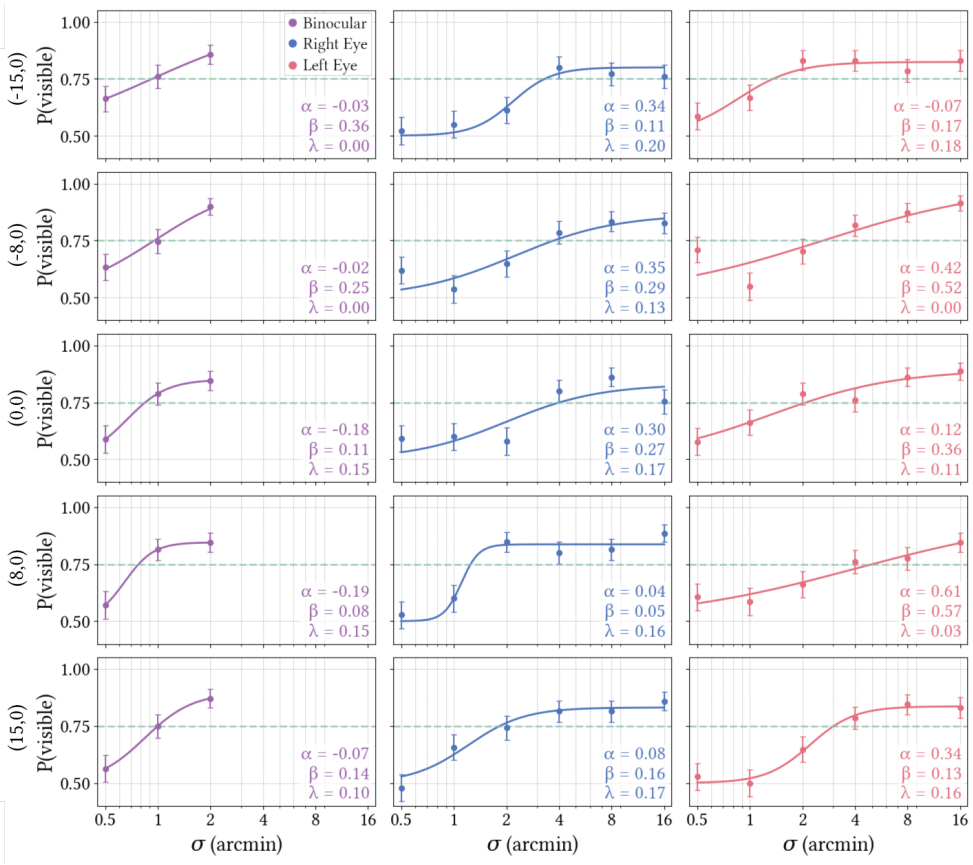

Fig. 10. Psychometric curves from Exp. 1 (horizontal fixation locations) showing the mean success rate $P(\text{visible})$ as a function of blur strength σ (arcmin), averaged across participants and trials (error bars denote SEM). The horizontal dashed line indicates $P = 0.75$, corresponding to reliable blur detection. The x-axis is shown on a logarithmic scale with ticks at the tested σ levels (0.5, 1, 2, 4, 8, and 16 arcmin). Parameter boxes report the fitted values of α, β, and λ.

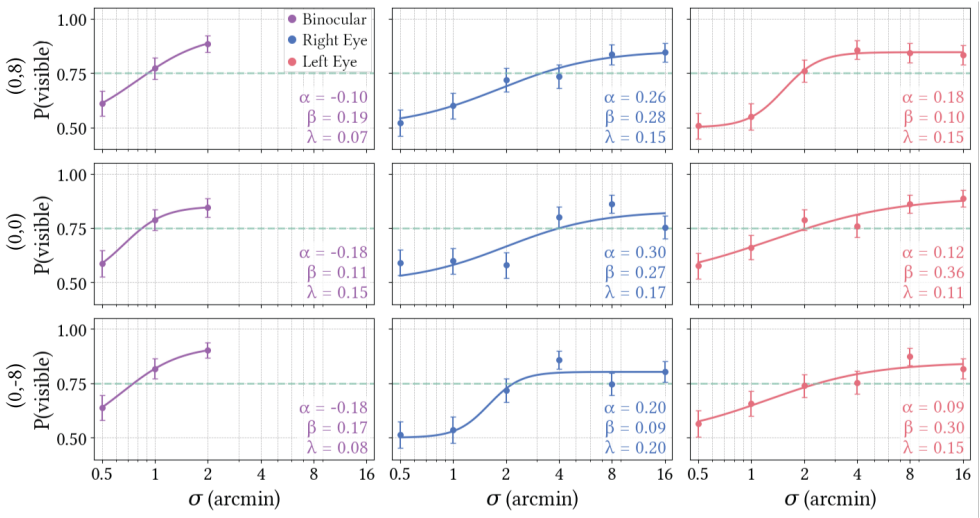

Fig. 11. Psychometric curves from Exp. 1 (vertical fixation locations) showing the mean success rate $P(\text{visible})$ as a function of blur strength σ (arcmin), averaged across participants and trials (error bars denote SEM). The horizontal dashed line indicates $P = 0.75$, corresponding to reliable blur detection. The x-axis is shown on a logarithmic scale with ticks at the tested σ levels (0.5, 1, 2, 4, 8, and 16 arcmin). Parameter boxes report the fitted values of α, β, and λ.